Visible thermochromism in vanadium pentoxide coatings

Sunil Kumar, Awais Qadir, Francis Maury, Naoufal Bahlawane

Visible Thermochromism in Vanadium Pentoxide Coatings

Sunil Kumar,[†] Awais Qadir,[†] Francis Maury,[‡] and Naoufal Bahlawane*[,†]

[†]Luxembourg Institute of Science and Technology (LIST), 5 avenue des Hauts-Fourneaux, L-4362 Esch-sur-Alzette, Luxembourg
[‡]CIRIMAT, ENSIACET-4 allée E. Monso, 31030 Toulouse, France

ABSTRACT: Although di-vanadium pentoxide (V_2O_5) has been a candidate of extensive research for over half a century, its intrinsic thermochromism has not been reported so far. Films of V_2O_5 grown on silicon, glass, and metal substrates by metal organic chemical vapor deposition in this study exhibit a thermally induced perceptible color change from bright yellow to deep orange. Temperature-dependent UV−vis spectroscopy and X-ray diffraction allow the correlation between the reversible continuous red shift of the absorption and the anisotropic thermal expansion along the (001) direction, that is, perpendicular to the sheets constituting the layered structure. Furthermore, the possibility of tuning the thermochromic behavior was demonstrated via a chemical doping with chromium.

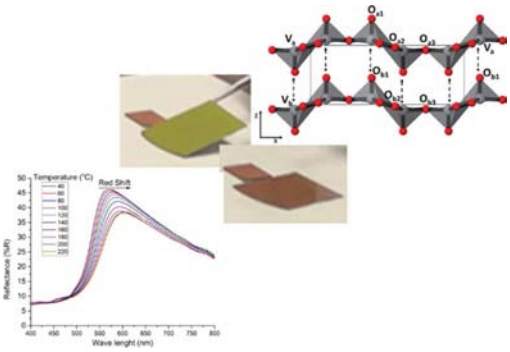

KEYWORDS: *Reversible thermochromism, di-vanadium pentoxide, MOCVD, functional oxide, smart coatings, polycrystalline films, temperature sensing, anisotropic lattice expansion*

INTRODUCTION

Thermochromism is a perceptible phenomenon, in many materials and compounds,[1] in which a change in color is observed as a response to a variation of temperature over a small or large range. This process involves thermally induced lattice expansion or change in the ligands, molecular structure, or coordination number.[2,3] Thermochromic materials find applications in a variety of fields ranging from simple decorative showpieces or toys to potentially breakthrough technological applications including comfort, lifesaving, and safety devices such as smart windows and sensors.[4,5]

Thermochromism might be reversible[6−9] or irreversible.[10,11] Reversible thermochromic materials, which restore their original color once the temperature stimulus is withdrawn, are useful temperature indicators. Everyday products, such as a cooking pan, can be coated with a thermochromic paint to indicate the attainment of the cooking temperature by visual cues.[12,13] Change in optical properties, if occurring in the visible spectral range, offers a considerable advantage and ease of detection. Reversible thermochromism can be further classified into two types that contrast in the accuracy of determining the temperature:

(a) Continuous thermochromism[14] takes place over a relatively wide range of temperatures. The change of the optical properties is then attributed to a gradual structural modification in the solid.
(b) Discontinuous thermochromism[15] occurs abruptly and corresponds to a change in the structure, for example, consequence of a ring opening and closing mechanism in polymer chains at a specific temperature.[16]

The color transitions in irreversible thermochromic materials typically results from decomposition, phase transition, or phase separation.[17,11] Irreversible thermochromism is useful in situations in which it is necessary to keep trace of the change in temperature even after the temperature stimulus has been withdrawn. Few examples include packaging labels of temperature-sensitive drugs or perishable food items, which indicate whether, for example, the cold chain integrity was compromised.[18−20] The irreversibility in thermochromism can be attributed to either thermodynamic or kinetic hindrance of the transformation.

Table 1 illustrates the different material groups that feature thermochromic behavior along with the transition temperature, the mechanism that leads to thermochromism, and the extent of reversibility. Thermochromic materials can be broadly categorized as organic and inorganic compounds.

Organic thermochromic compounds include the following:

Conjugated polymers[21] − Thermochromism arises due to the conformational change, which influences the effective conjugation length of the polymer backbone. A slight change in the structure usually leads to a significant color shift. Some examples for each category are discussed hereafter:

Bianthrones[1] − With the increase in temperature, the central double bond expands and weakens, allowing the two noncoplanar anthrone moieties to rotate in their planes, thus enabling stereoisomerism with a consequent thermochromism.

Schiff bases[6,22] − Proton transfer is the basis of thermochromic behavior in many metal Schiff's base complexes. The shift in the keto−enol equilibrium, caused by the thermally

Table 1. Overview of Various Thermochromic Materials with Their Working Mechanisms and Operation Temperature

type	mechanism of thermochromism	temperature range of operation (°C)	nature of transition	decomposition temperature (°C)	examples	references
			Organic Compounds			
liquid crystals	variation in the crystal field and Bragg's reflection	−30 to 120	reversible	130−150	cholesterol esters	12, 24, 25
leuco dyes	change of molecular structure	−100 to 200	reversible	>200	fluorans or crystal violet lactone, spiropyrans, or fulgides	
conjugated polymers	conformational change of polymer backbone	70−350	both reversible and irreversible	>400	polydiacetylenes or polythiophenes	21
bianthrones	sterioisomerism	80−300	reversible	>300	bianthrones and highly crowded ethylenes	1
Schiff's base and acids	hydrogen ion transfer	60−300	both reversible and irreversible	>400	nickel(II) and copper(II) complexes of Schiff bases derived from 8-aminoquinoline	6, 22
			Inorganic Compounds			
metal salts	phase transition and change in ligand geometry or coordination	100−200	both reversible and irreversible	>300	Cu_2HgI_4, Ag_2HgI_4, and AgI	3, 15
metal oxides		50−800	reversible	>800	TiO_2, VO_2, ZnO, WO_3, $NiCO_2$, Nh_4VO_3, and $NiMoO_4$	

influenced pH change, is the fundamental aspect of color change.

Spiropryans and Spirooxazines[16,23] − Thermally induced molecular rearrangements lead to the change of the Spiro carbon hybridization from sp^3 to sp^2. This change is accompanied by a large delocalization of the electron density, giving rise to electron transitions that fall in the visible region of the spectrum, thus producing color and color change.

Leuco dyes and liquid crystals[12,24,25] − In a cholesteric liquid crystal, changes in temperature result in thermal expansion, which leads to a change in layer spacing and the angle of rotation with a consequent color change. Because the pitch varies continuously as the temperature changes, a continuous thermochromism is expected in such compounds. Liquid crystals and leuco dyes have to be microencapsulated for them to be used for coloration. This includes embedding them in a shell material.

Inorganic thermochromic compounds consist of *metal salts and metal oxides*. The mechanisms of color change include temperature-dependent changes in ligand geometry, change in metal coordination, variation of band-gap energy, the arrangement and distribution of defects in the crystalline solid, and most importantly through phase transitions occurring in the material.[3,15]

Among the plethora of thermochromic materials, inorganic compounds provide the advantage of being stable at high temperatures when compared with their organic counterparts. Because inorganic materials are generally much more resistant to photo-induced decomposition than the organic counterparts, they feature substantially extended lifetimes. Furthermore, the preparation of powders, pigments, or films based on inorganic compounds is more convenient owing to their ease of handling and robustness. As most inorganic thermochromism results from lattice expansion, perceptible change in color can be observed even at elevated temperatures.[26]

Metal oxides act in general as semiconductors showing a decrease in electrical resistivity with temperature. Hence, metal oxide compounds featuring a wide band gap semiconducting property, which also exhibits a continuous visible range thermochromism over a wide temperature window, could be ideal candidates for many thermo-electro-optical applications. In this context, Yu et al.[27] developed an adaptive optoelectronic camouflage on the basis of the integration of thermochromic dyes with arrays of actuators and photo-detectors laminated on transparent and flexible substrates. A second example is reported by Kim et al.,[28] demonstrating the mechanism and performance of a resistive pressure sensor and its integration into a dynamic and interactive thermochromic panel.

Oxides of vanadium are very popular for their chromic behavior due to the numerous oxidation states of vanadium: +5, +4, +3, and +2, easily distinguishable by their contrasting optical properties. Vanadium pentoxide (V_2O_5) with an oxidation state of +5 is by far the most studied phase.[29−31] V_2O_5 has an orthorhombic layered structure that can host small guest molecules or ions. Because of this property, V_2O_5 is intensively investigated as a catalyst for organic reactions[32] and also finds use in lithium ion batteries,[33] gas sensors,[34] electrochromism,[35] and photochromism.[36] Nevertheless, there is a wide inconsistency when it comes to the description of the physical color of V_2O_5 at room temperature. The reported colors of the compound range from yellow, yellow-to-red, or rust brown or orange.[37−39]

In addition, there seems to be no previous report on the thermochromic behavior of pure V_2O_5. Lataste et al. reported the implementation of V_2O_5 as a mixture in pigments to alter the thermochromic behavior of barium carbonate.[40] In a study by Gaudon et al. reporting the use of an inorganic material blend to mimic the red-to-green transition,[41] the V_2O_5 powder was blended with Cr_2O_3 to investigate the thermally induced color change. Surprisingly, the intrinsic thermochromic behavior of V_2O_5 seems to be overlooked. It should be cautiously noted that another oxide of vanadium, namely VO_2, is extensively studied for its thermochromic behavior in the infrared spectral range,[42] but we strictly restrict this study to V_2O_5 for all purposes. In this work, we shed light on the intrinsic visible thermochromism in pure and chemically doped vanadium pentoxide (V_2O_5) thin films at elevated temperatures.

EXPERIMENTAL SECTION

Deposition Process. Thin films of vanadium oxide were deposited on silicon substrates by direct liquid injection (DLI) metal organic chemical vapor deposition (MOCVD) in a custom-built warm wall vertical stagnation point flow reactor. A low-concentration (5×10^{-3} M) ethanol solution of 99.9% pure vanadium (V) oxy-tri-isopropoxide [$VO(O^iPr)_3$] was used as the precursor feedstock. Liquid injection was performed in an evaporation tube maintained at 225 °C to secure the quasi instantaneous vaporization of the precursor solution. The injection was maintained at 4 Hz with a 4 ms opening time resulting in a liquid flow rate of 1.33 mL/min. Argon was used as the carrier gas at a flow rate of 50 cm^3/min, while the chamber pressure was adjusted to

10 mbar. Substrates were maintained at a constant temperature of 500 °C during the 4 h of deposition.

After deposition, the samples were allowed to cool to room temperature in an argon atmosphere under low pressure before withdrawing from the chamber and further handling under an ambient atmosphere. A postdeposition anneal was performed under ambient air at 450 °C.

A series of Cr-doped V_2O_5 thin films was also grown by the implementation of mixed precursor feedstock with an adjusted Cr/V ratio. Doping V_2O_5 films with Cr was achieved by simply mixing at various dilutions a 5 mM ethanol solution of chromium acetylacetonate, $Cr(acac)_3$, into the vanadium precursor used for the MOCVD deposition.

Thin Film Characterization. X-ray diffraction (XRD) was used to characterize the films using the Bruker D8, with Cu Kα as the X-ray source. Data were collected in the $\theta-2\theta$ (locked couple) mode from 2θ of 10−30° with a step size of 0.02°. Temperature-dependent XRD was performed using a heated stage with an integrated thermocouple and air cooling for temperature regulation. The film thickness was measured using an α step d-500 Profilometer from KLA-Tencor and the cross-section inspection with FEI Helios Nanolab 650 scanning electron microscopy (SEM). Surface and cross-sectional morphologies were characterized by SEM at a working distance of 4 mm with an acceleration voltage of 25 kV.

Raman scattering was performed using an InVia Raman spectrometer from Renishaw with a 532 nm laser at 0.2 mW to avoid noncontrolled surface heating. Optical reflectivity measurements were carried out on a LAMBDA 1050 UV/vis/NIR spectrophotometer from PerkinElmer with a 100 mm integration sphere in the reflection configuration. Measurements were performed in the visible spectral range (400−800 nm). For both spectroscopies, in situ measurements at variable temperatures were carried out under an ambient atmosphere. For technical reasons related to the apparatus, we restrict the UV−vis measurements to a maximum temperature of 220 °C.

RESULTS AND DISCUSSION

Undoped V_2O_5 Thin Films. The film deposition parameters, like temperature and pressure, were adjusted to achieve highly porous nanocrystalline films with mixed crystalline phases of vanadium oxide VO_x. Deposition conditions were chosen on the basis of a previously reported systematic study.[43] With an average growth rate of 10 nm/min, a 4 h deposition yields a 2.4 μm thick film (Figure 1).

Temperature-dependent XRD and Raman scattering provide evidence that annealing of the as-grown VO_x films under ambient air at 450 °C for 10 min allows the complete oxidative conversion of the films to pure V_2O_5. This is in good agreement with the temperature range of 450−550 °C previously reported to be optimal for this purpose.[44] The oxidation process requires an extended time of annealing at lower temperatures. For example, 1 h is needed when the annealing temperature is 300 °C. The oxidation of vanadium occurs due to the gas−solid reaction, followed by oxygen diffusion into the film. It is worth mentioning that the porous structure of the film (Figure 1) has a clear advantage in this respect. The aforementioned post-treatment results in the formation of a thermodynamically preferred phase, which is the layered orthorhombic V_2O_5 with the *Pmmn* space group.[45]

Figure 1a,b displays the surface and cross-section micrographs of as-deposited films, which exhibit a highly nanoporous structure. Upon oxidation, grains coalesce, grow in size, and exhibit apparent sheet-like terraces. The porosity of the films is retained, as shown in the surface and cross-section micrographs in Figure 1c,d, respectively. The layered sheet-like morphology

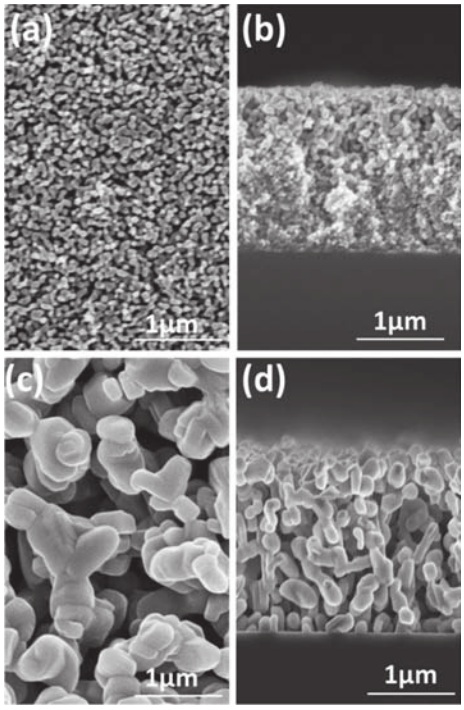

Figure 1. Surface (a, c) and corresponding cross-section (b, d) micrographs of as-deposited (VO_x)/annealed (V_2O_5) films, respectively.

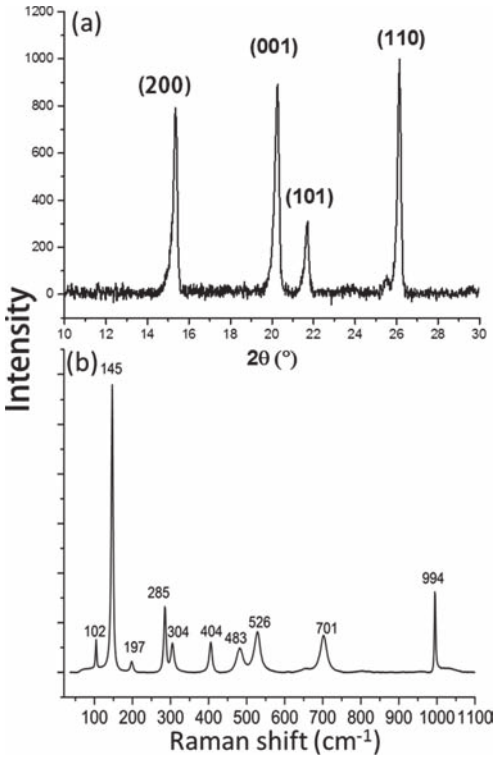

Figure 2. (a) X-ray diffractogram and (b) Raman spectrum of the oxidized films indicating the formation of a single-phase V_2O_5 film. Panel (a) corresponds to Miller indices of the diffraction peaks, attributed to the orthorhombic V_2O_5 per PDF no [00-041-1426]. Each indicated peak in the Raman spectrum corresponds to V_2O_5.

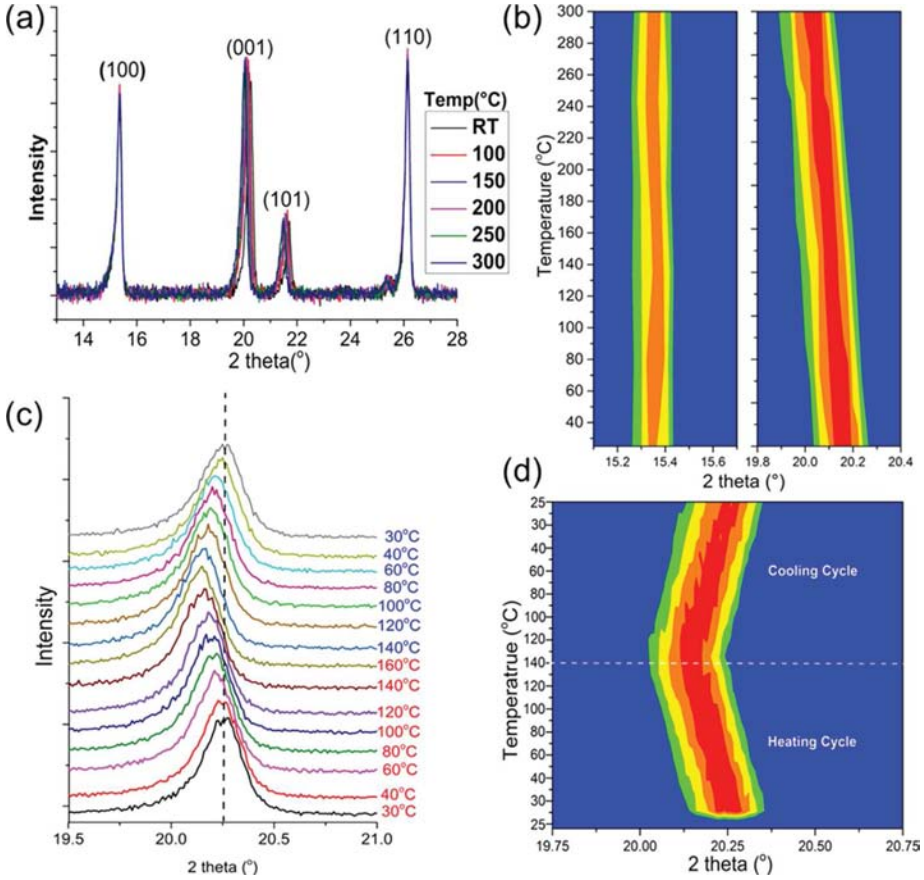

Figure 3. (a) Temperature-dependent XRD of the V_2O_5 film and (b) contour plot of the peaks corresponding to (200) and (001) reflexes. Notice the peak of (001) orientation shifting gradually with increasing temperatures. Both contour plots correspond to $\Delta(2\theta) = 0.6°$. The reversibility of the thermochromism is monitored in (c) and (d) by measuring the shift of the reflex (001) in the heating and cooling stages.

of the grains shown in Figure 1c is characteristic of orthorhombic V_2O_5.[46,47]

X-ray diffraction and Raman spectroscopy of the oxidized films, shown in Figure 2, reveal the single-phase pure V_2O_5 nature of the resulting films from the oxidative postannealing. The presence of all expected XRD peaks indicates the polycrystalline nature of the film. The comparison of their relative intensities with those of randomly oriented V_2O_5 powder given by the PDF file 00-041-1426 does not reveal any apparent preferred orientation even if the (200) peak is slightly more intense than that in the standard. The porous morphology of the coating favors the random orientation of the small crystallites. The average crystallite size calculated using Scherrer's formula from the XRD spectra is approximately 50 nm. Raman vibrational peaks observed at 102, 197, 304, 404, 483, 526, and 994 cm^{-1} belong to the A_g vibrational modes, whereas peaks observed at 145, 285, and 701 cm^{-1} belong to the B_g modes of V_2O_5.[46,48]

Two strategies were adopted to thermally oxidize the as-deposited films. Samples were either heated gradually from room temperature to 450 °C using a heating ramp of 10 °C/min and then maintained at 450 °C for 10 min (first route) or subjected to an instantaneous heat at 450 °C in ambient air for 10 min (fast oxidation route). During the oxidation process, the color of the VO_x films changed from dark gray to deep red-orange. No further perceptible change in color was observed even after extended periods, indicating the complete oxidation to V_2O_5. Both oxidation approaches yield XRD-pure V_2O_5 films that are orange at a high temperature and yellow at room temperature. The gradually oxidized films feature a glossy appearance and resist scratching when compared with the matte films obtained through fast oxidation. Therefore, the systematic investigation was limited to films obtained through gradual oxidation.

Temperature-dependent XRD was performed under an ambient atmosphere in the 25−300 °C range. It is interesting to notice from Figure 3 that, although the peak positions and intensity remain constant, the peak corresponding to the (001) orientation shows a regular and reversible shift toward low diffraction angles with increasing temperatures. This shift is a clear indication of the anisotropic expansion of the lattice along the "*c*" direction.

The contour plots in Figure 3b clearly show the (001) peak shifting gradually toward low values of 2θ upon heating, whereas the (200) peak remains unaffected. On cooling to room temperature, the reverse shift occurs uniformly without any hysteresis effect, as shown in Figure 3c,d. Figure 4 shows the variation in the calculated lattice parameters from the XRD data as a function of temperature. Whereas the lattice parameters "*a*" and "*b*" remain unchanged, the parameter *c* features a linear increase with the temperature.

Some oxides of vanadium are well known for their semiconductor−metal transition (SMT), the occurrence of which in V_2O_5 has been suggested by few authors.[49,50] Recent

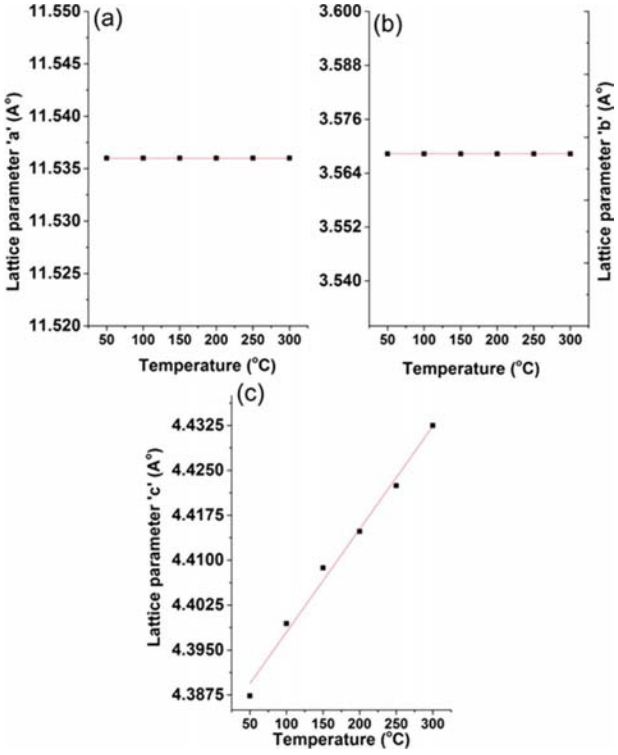

Figure 4. Variation of V_2O_5 lattice parameters *a*, *b*, and, *c* with respect to temperature. Lattice parameters *a* and *b* are insensitive to the temperature, whereas the parameter *c* features a linear increase with the temperature.

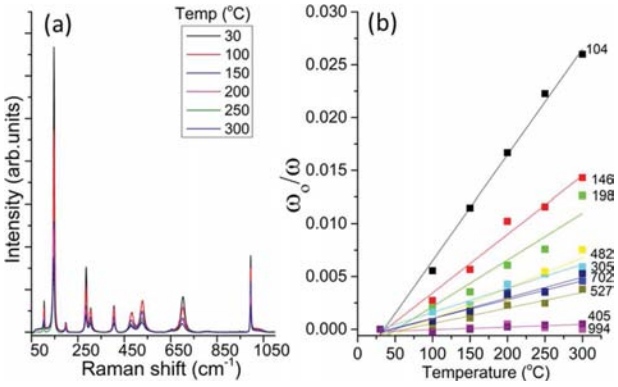

Figure 5. (a) Temperature-dependent Raman scattering of pure V_2O_5 films. (b) Raman shift for each individual vibrational mode with respect to the increasing temperature (w_0 is the frequency at 30 °C).

studies disagree, however, with this suggestion.[51,52] The change in electrical conductivity, interpreted as SMT,[49,50] was attributed to irreversible surface-limited reduction of V_2O_5 to V_6O_{13} due to the ultrahigh vacuum conditions encountered for the analysis.[51,52] The rate of this reduction is further enhanced by electron beam or X-ray irradiation. From both Raman and XRD analysis over a wide range of temperatures, it is evident in our study that the V_2O_5 films remain pure under ambient air and show no signs of reduction at elevated temperatures.

Temperature-dependent Raman spectroscopy, displayed in Figure 5a, reveals a red shift of the Raman vibration modes due to thermal expansion. A relative frequency shift (w_0/w, where

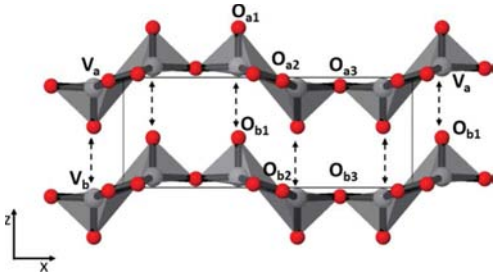

Figure 6. Illustration of the V_2O_5 lattice showing the layered sheet-like structure. Individual sheets are held together by the weak V_a-O_{b1} and V_b-O_{a1} interactions.

w_0 is the frequency at 30 °C) for each vibrational mode is plotted as a function of temperature in Figure 5b. This shift shows which bonds undergo modifications due to thermal excitation.

V_2O_5 has a layered structure, as illustrated in Figure 6. For the sake of convenience, let us name the sheets shown as layer "A" and layer "B". The vanadium and oxygen atoms for sheet A are denoted as V_a and O_a and those of sheet B are V_b and O_b. Each unit cell comprises VO_5 square pyramids. These pyramids have O_{a1}/O_{b1} at their apexes and are connected through their bases either by sharing edges, involving O_{a2}/O_{b2} oxygen ions, or vertices, by involving O_{a3}/O_{b3} oxygen ions. Lattice parameter *c* equals to the sum of the bond lengths V_a-O_{a1} and V_a-O_{b1}. Raman analysis with respect to temperature reveals no impact on the peak position at 994 cm^{-1}. This corresponds to the stretching of V_a-O_{a1} or V_b-O_{b1} bonds. Hence, we can conclude that the bond length between V and O from the top of the pyramid does not change as the temperature increases. However, we do notice an increase in lattice parameter *c* from the XRD analysis. This means that, whereas the bond length of V_a-O_{a1} remains constant, there is an increase in the bond length of V_a-O_{b1} and V_b-O_{a1} exclusively. Therefore, an expansion in the (001) direction can be visualized as if individual sheets are moving apart from each other due to the elongation of the weak bonds holding the two sheets in place, thus expanding the interlayer space.

This kind of anisotropic expansion enables the V_2O_5 lattice to host ions with important application in energy storage, sensing, and electrochromism.[35]

The total hemispherical reflectance measured in the range from 400 to 800 nm as a function of temperature (Figure 7) indicates a thermochromic behavior of V_2O_5. A clear red shift is witnessed with the increasing temperature. This shift is also reversible over the entire range of temperature from 25 to 450 °C. The measured THR values during the heating and cooling stages coincide with differences in the third decimal. The film is a single-phase crystalline V_2O_5 as confirmed by Raman and XRD analyses. Therefore, Figure 7 represents the first demonstration of the visible gradual thermochromism in pure crystalline V_2O_5 films.

The optical band gap, E_g, was calculated as a function of temperature using the temperature-dependent reflectance spectra, by Tauc's equation, $\alpha h\nu = B(h\nu - E_g)^r$, where α is the absorption coefficient, E_g is the optical energy gap of the film, *B* is a constant, $h\nu$ is the incident photon energy, and *r* is a numeric value equal to 1/2 for allowed direct transitions and 2 for allowed indirect transitions. The optical energy gap is estimated by plotting $(\alpha h\nu)^{1/r}$ versus $(h\nu)$ and then interpolating the straight line to the photon energy axis at

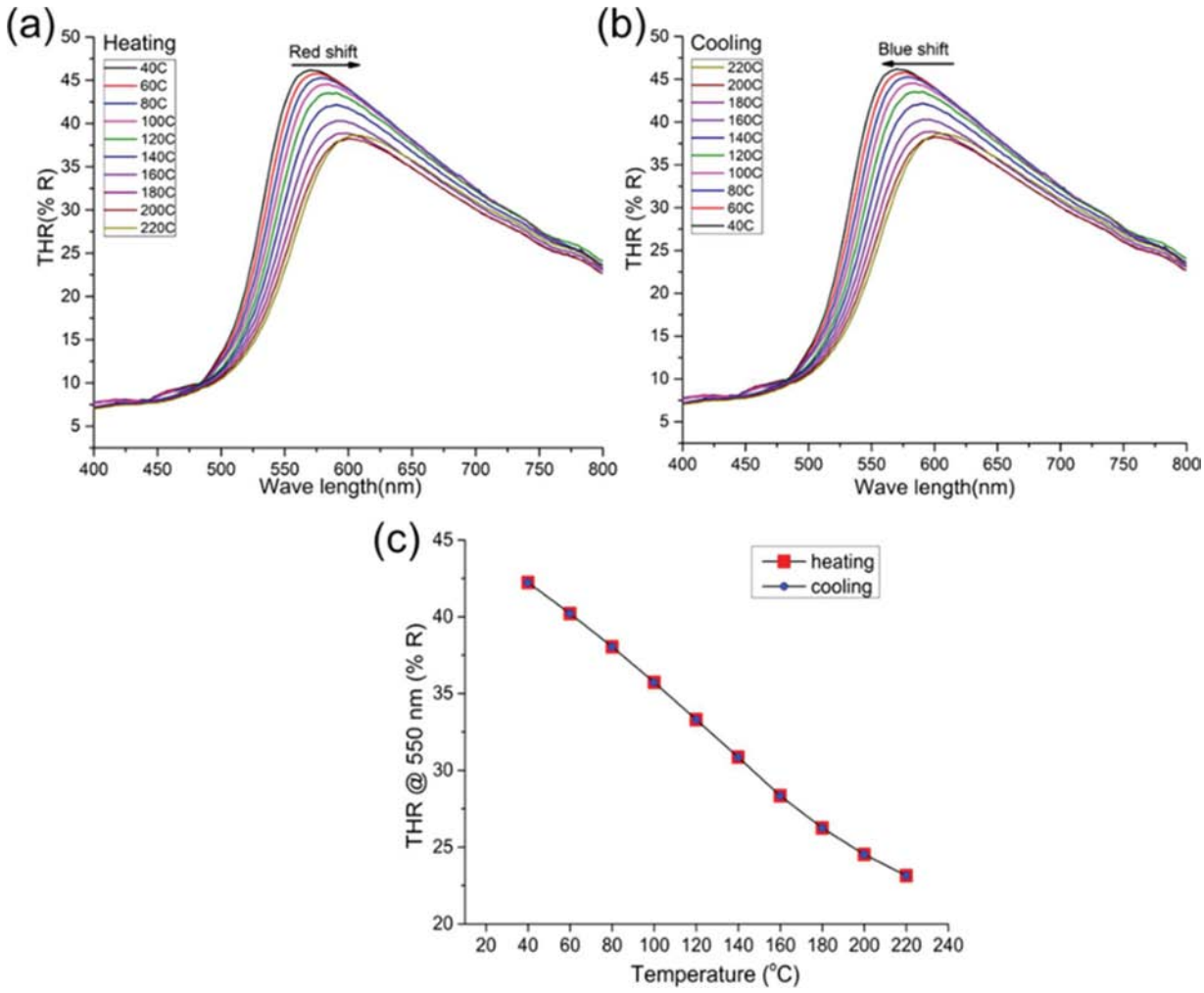

Figure 7. Temperature-dependent total hemispherical reflectance (THR in %) for V_2O_5 films under an ambient atmosphere during (a) heating and (b) cooling stages. (c) THR at 550 nm plotted vs temperature during the heating and cooling cycles.

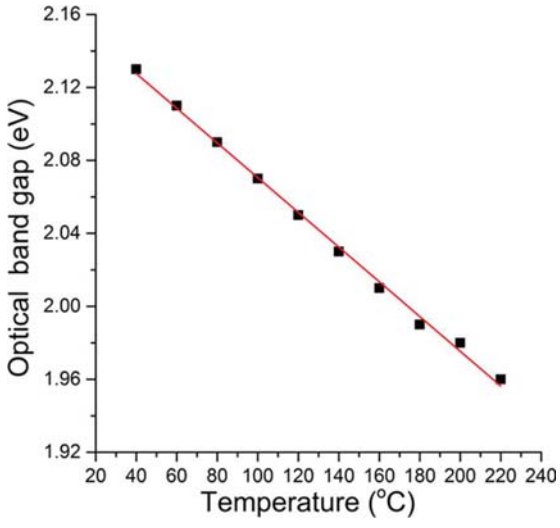

Figure 8. Optical energy band gap calculated as a function of temperature from the reflectance spectra.

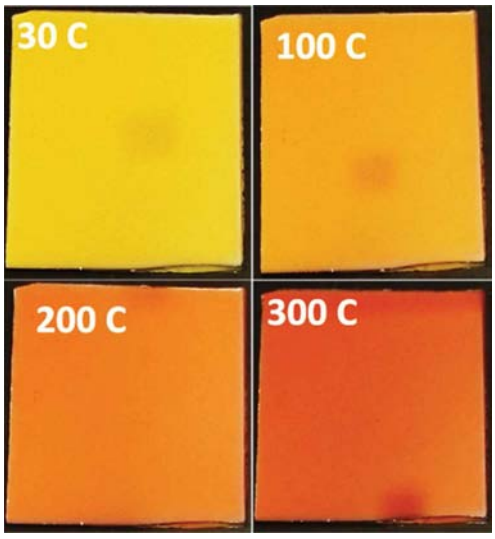

Figure 9. Photographs taken at different temperature intervals of the coated silicon substrate with V_2O_5 films in an ambient atmosphere.

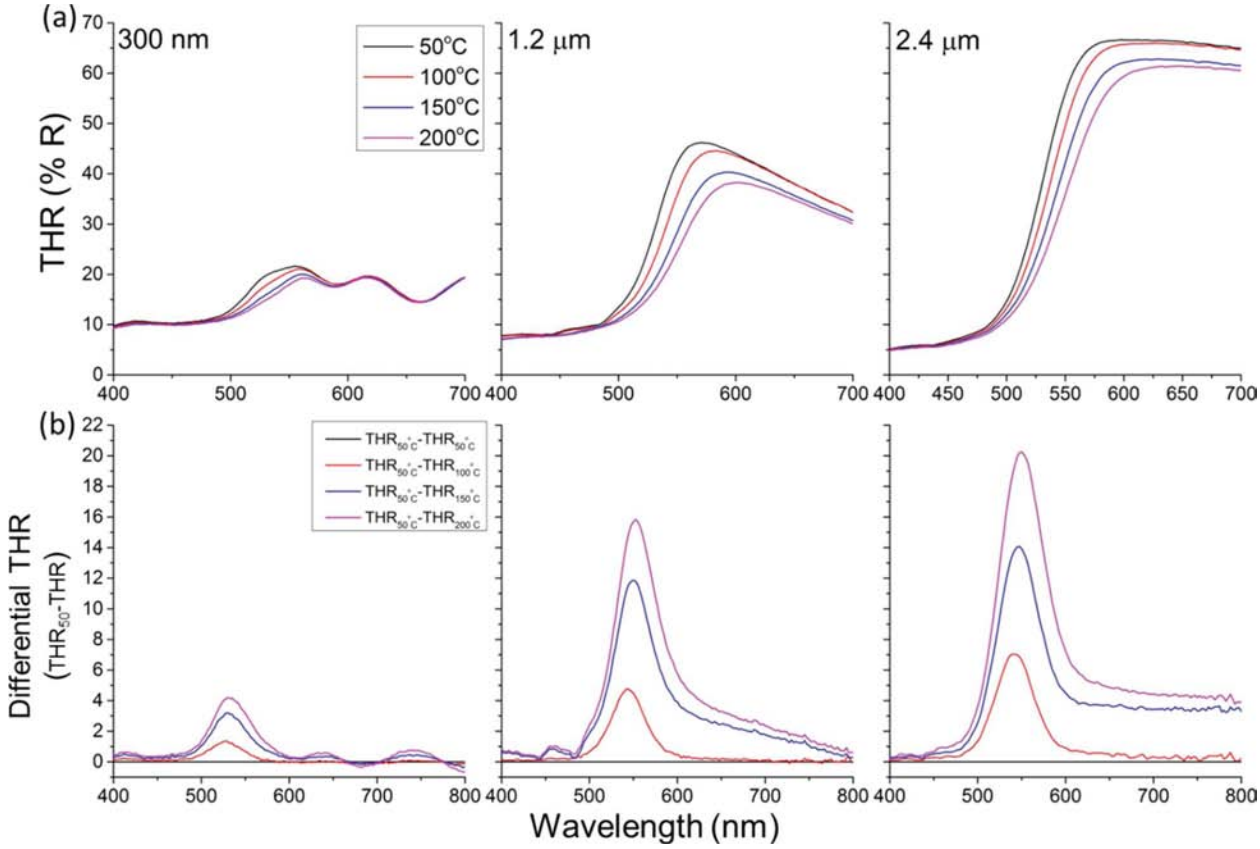

Figure 10. (a) Temperature-dependent THR for various thicknesses (0.3, 1.2, and 2.4 μm) of V_2O_5 films on silicon substrates and (b) the differential spectra referring to the obtained spectra at 50 °C.

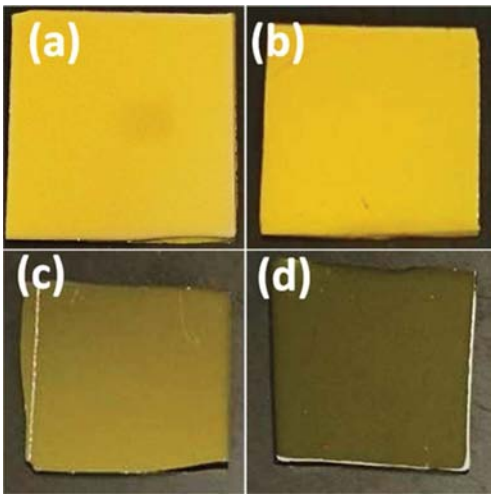

Figure 11. Photographs of (a) undoped V_2O_5 and (b) 0.21%, (c) 2.41%, and (d) 4.34% Cr-doped V_2O_5 at room temperature.

the value $(\alpha h\nu)^{1/r} = 0$. The obtained data for vanadium pentoxide films were found to give a better fit for the exponent, $r = 1/2$, confirming the direct allowed nature of the involved transition. The calculated optical band gap of 2.13 eV at room temperature is in good agreement with the values reported in the literature for allowed direct band gap excitations in V_2O_5.[53] A gradual decrease in the optical band gap is observed when V_2O_5 is heated (Figure 8). This observation correlates with the lattice expansion in the (001) direction observed in the XRD analysis (Figure 4).

Figure 9 evidences the thermochromism of V_2O_5-coated silicon substrates. A change of color from bright yellow to deep orange is observed as the temperature increases under ambient air. This behavior is robust and highly reproducible. The V_2O_5 layers are highly stable and do not undergo reduction into other oxides of vanadium under an ambient atmosphere at elevated temperatures. This high thermal stability of the thermochromic coating is noteworthy. This thermochromic behavior persists even when the V_2O_5 layer was encapsulated by a thin transparent layer of 20 nm of Al_2O_3 to avoid the interaction with ambient air.

The thermochromic behavior of V_2O_5 films with various thicknesses was investigated to clarify the potential attribution of the thermochromism to the extreme surface state. The results displayed in Figure 10a highlight various aspects. The observed reflectance below λ = 500 nm weakens for thicker films, suggesting its association with the substrate behavior. The reflectance above this wavelength strengthens considerably with the increased V_2O_5 film thickness, which is a clear evidence of its attribution to the coating. Thermochromism of V_2O_5, red shift of the film's reflection edge with the increased temperature, is observed regardless of the film thickness. The amplitude of the red shift remains unchanged, as shown in Figure 10b, and the differential spectra show maxima at wavelengths that depend on the temperature and not the thickness of the film. The intensity of the differential spectra features a considerable enhancement with the thickness of the

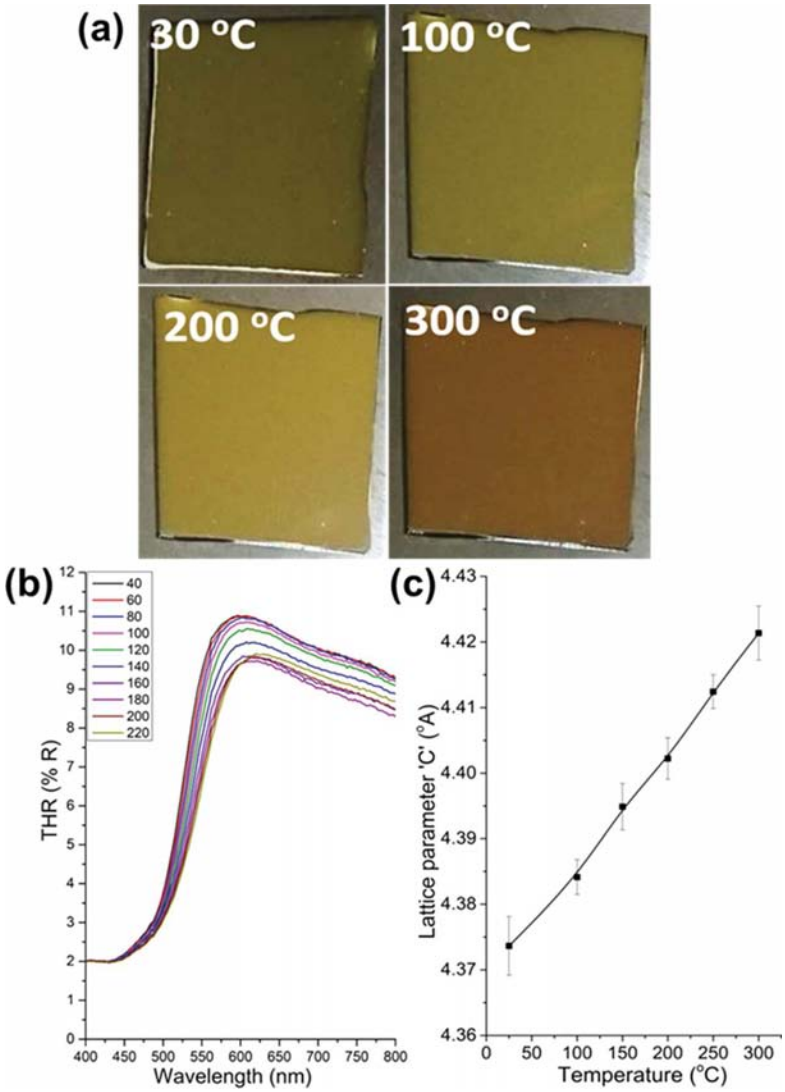

Figure 12. (a) Photographs of 4.34% Cr-doped V_2O_5 at different temperatures, (b) the temperature-dependent THR, and (c) lattice parameter *c*.

film, which hints at the contribution of the bulk of the film to the thermochromism of V_2O_5.

Cr-Doped V_2O_5 Thin Films. The thermochromic nature is itself an appealing property for the already popular and multifunctional V_2O_5. Providing means to tune the optical properties of the thermochromic V_2O_5 is advantageous to tailor the optical response to specific wavelengths or constrain to certain temperature windows. Chemical doping offers a convenient way to alter film properties. Initial demonstration was performed by chromium incorporation into the lattice.

Three different Cr doping levels were attained in the V_2O_5 films, having a Cr atomic concentration in the film of 0.21, 2.41, and 4.23%, respectively. A noticeable change in the perceived color at room temperature results from the Cr doping of V_2O_5. As shown in Figure 11, films with a Cr doping concentration of 0.21% appear very similar to nondoped films, owing to the very low doping concentration. Nevertheless, as the doping level increases to 2.41 and 4.23%, the color of the films changes progressively to mustard yellow and olive green, respectively, as shown in Figure 11b,c.

The impact of temperature on the Cr-doped films is shown in Figure 12a for the doping concentration of 4.34%. A perceptible color change is observed. Although not as impressive as for nondoped V_2O_5, Cr-doped films feature a thermochromism with colors that differ from those of the parent material. A higher concentration of doping has not resulted in any further perceptible color change. Temperature-dependent THR and change of lattice parameter *c*, displayed in Figure 12b,c, respectively, reveal no abrupt changes in the structure or optical properties.

The XRD patterns and Raman spectra of Cr-doped films, not shown here, remain unchanged at room temperature. They look identical to pure V_2O_5 films with no measurable alteration of the crystal structure.

Highly porous films comprising orthorhombic V_2O_5 hold the key for perceptible thermochromism. Chemical doping has clearly shown its impact on the tunability of this thermochromism. Other doping elements are expected to further extend the tunability of the optical properties in V_2O_5 films.

CONCLUSIONS

Pure single-phase and polycrystalline films of vanadium pentoxide (V_2O_5) were synthesized by thermal oxidation of as-grown VO_x films with DLI-MOCVD. The resulting films exhibit excellent reversible and continuous thermochromism from bright yellow at room temperature to deep orange at elevated temperatures. Although V_2O_5 functionality was evidenced for a wide variety of applications, thermochromism has never been reported till date. Temperature-dependent XRD and Raman confirm the absence of any kind of abrupt changes or phase transitions, and the bulk of the film was shown to contribute to the observed thermochromism. A regular anisotropic thermal expansion of the lattice along the (001) direction was observed, that is, perpendicular to the sheets constituting the structure and correlated with the observed thermochromism. Tuning the thermochromic behavior was also investigated. Cr doping was successively used to alter the perceived color of V_2O_5 at ambient and elevated temperatures. This study opens up additional opportunities and application possibilities with V_2O_5 as a thermochromic material.

AUTHOR INFORMATION

Corresponding Author

*E-mail: naoufal.bahlawane@list.lu.

ORCID

Naoufal Bahlawane: 0000-0003-1094-2512

Notes

The authors declare no competing financial interest.

REFERENCES

(1) Day, J. H. Thermochromism. *Chem. Rev.* **1963**, *63*, 65−80.

(2) Samat, A.; Lokshin, V. Thermochromism of Organic Compounds. In *Organic Photochromic and Thermochromic Compounds*, Springer US, 2002; Vol. 2, pp 415−466.

(3) Day, J. H. Thermochromism of Inorganic Compounds. *Chem. Rev.* **1968**, *68*, 649−657.

(4) Blaney, T. S.; Plugs, B. Sink and Bath Plugs. U.S. Patent US6105618 A, 2000.

(5) Lerner, W. Method of Warning Individuals About Hot Surfaces on Stoves Including Cooktops. U.S. Patent Application 10/658,214, 2003.

(6) Grzybowski, M.; Gryko, D. T. Diketopyrrolopyrroles: Synthesis, Reactivity, and Optical Properties. *Adv. Opt. Mater.* **2015**, *3*, 280−320.

(7) Guo, H.; Zhang, J.; Porter, D.; Peng, H.; Löwik, D. W. P. M.; Wang, Y.; Zhang, Z.; Chen, X.; Shao, Z. Ultrafast and Reversible Thermochromism of a Conjugated Polymer Material Based on the Assembly of Peptide Amphiphiles. *Chem. Sci.* **2014**, *11*, 4189−4195.

(8) Wei, R.; Panshu, S.; Aijun, T. Reversible Thermochromism of Aggregation-Induced Emission-Active Benzophenone Azine Based on Polymorph-Dependent Excited-State Intramolecular Proton Transfer Fluorescence. *J. Phys. Chem. C* **2013**, *117*, 3467−3474.

(9) Gaudon, M.; Deniard, P.; Demourgues, A.; Thiry, A. E.; Carbonera, C.; Le Nestour, A.; Largeteau, A.; Létard, J. F.; Jobic, S. Unprecedented "One-Finger-Push" -Induced Phase Transition with a Drastic Color Change in an Inorganic Material. *Adv. Mater.* **2007**, *19*, 3517−3519.

(10) Koshihara, S. Y.; Tokura, Y.; Takeda, K.; Koda, T.; Kobayashi, A. Reversible and Irreversible Thermochromic Phase Transitions in Single Crystals of Polydiacetylenes Substituted with Alkyl-Urethanes. *J. Chem. Phys.* **1990**, *92*, 7581−7588.

(11) Rougeau, L.; Picq, D.; Rastello, M.; Frantz, Y. New Irreversible Thermochromic Polydiacetylenes. *Tetrahedron* **2008**, *64*, 9430−9346.

(12) Lazaroff, W.; Raschdorf, A. Thermochromic Cookware. U.S. Patent Application 10/965,317, 2004.

(13) Pimia, J. Temperature Indicator for Temperature Changing Material or Means and Method for its Preparation. U.S. Patent Application 13/637,097, 2011.

(14) Petruševski, V. M.; Bukleski, M.; Monkoviæ, M. The Economic Demonstrator: Prepare it Once, Use it Many Times. II. Continuous Thermochromism In Aqueous Solutions Of Transition Metal Chlorides. *Chemistry* **2007**, *16*, 20−26.

(15) Petruševski, V. M.; Bukleski, M. The Economic Demonstrator: Prepare It Once, Use It Many Times. III. Phenomena of Discontinuous Thermochromism. *Chemistry* **2008**, *17*, 109−117.

(16) Dorogan, I.; Minkin, V. Theoretical Modeling of Electrocyclic 2H-Pyran and 2H-1,4-Oxazine Ring Opening Reactions in Photo- and Thermochromic Spiropyrans and Spirooxazines. *Chem. Heterocycl. Compd.* **2016**, *52*, 730−735.

(17) Rougeau, L.; Picq, D.; Rastello, M.; Frantz, Y. New Irreversible Thermochromic Polydiacetylenes. *Tetrahedron* **2008**, *64*, 9430−9436.

(18) Parker, R. Time-Temperature Indicator. U.S. Patent 4,805,188, 1989.

(19) Parker, R. Expiration Indicator. U.S. Patent 7,188,996, 2007.

(20) Galliani, D.; Mascheroni, L.; Sassi, M.; Turrisi, R.; Lorenzi, R.; Scaccabarozzi, A.; Stingelin, N.; Beverina, L. Thermochromic Latent-Pigment-Based Time−Temperature Indicators for Perishable Goods. *Adv. Opt. Mater.* **2015**, *3*, 1164−1168.

(21) Yoon, S. J.; Kim, J. H.; Kim, K. S.; Chung, J. W.; Heinrich, B.; Mathevet, F.; Kim, P.; Donnio, B.; Attias, A. J.; Kim, D.; Park, S. Y. Mesomorphic Organization and Thermochromic Luminescence of Dicyanodistyrylbenzene-Based Phasmidic Molecular Disks: Uniaxially Aligned Hexagonal Columnar Liquid Crystals at Room Temperature with Enhanced Fluorescence Emission and Semiconductivity. *Adv. Funct. Mater.* **2012**, *22*, 61−69.

(22) Donia, A. M.; El-Boraey, H. A. Reversible and Irreversible Thermochromism of Some Schiff Base Metal Complexes. *Transition Met. Chem.* **1993**, *18*, 315−318.

(23) Bourque, A. Investigations of Reversible Thermochromism in Three-Component Systems. Ph.D. Thesis, Dalhousie University: Canada, 2014 (DC.identifier.uri: http:/hdl.handle.net/10222/49088).

(24) Sage, I. Thermochromic Liquid Crystals in Devices. In *Liquid Crystals — Applications and Uses*; World Scientific Publishing, 1992; Vol. 3, pp 301−343.

(25) White, M. A.; Leblanc, M. Thermochromism in Commercial Products. *J. Chem. Educ.* **1999**, *76*, 1201.

(26) Poole, C. P. The Optical Spectra and Color of Chromium Containing Solids. *J. Phys. Chem. Solids* **1964**, *25*, 1169−1182.

(27) Yu, C.; Li, Y.; Zhang, X.; Huang, X.; Malyarchuk, V.; Wang, S.; Shi, Y.; Gao, L.; Su, Y.; Zhang, Y.; Xu, H.; et al. Adaptive Optoelectronic Camouflage Systems with Designs Inspired by Cephalopod Skins. *Proc. Natl. Acad. Sci. U.S.A.* **2014**, *111*, 12998−13003.

(28) Kim, G.; Cho, S.; Chang, K.; Kim, W. S.; Kang, H.; Ryu, S. P.; Myoung, J.; Park, J.; Park, C.; Shim, W. Spatially Pressure-Mapped Thermochromic Interactive Sensor. *Adv. Mat.* **2017**, *29*, No. 1606120.

(29) Beke, S. A Review of The Growth of V_2O_5 Films From 1885 to 2010. *Thin Solid Films* **2011**, *519*, 1761−1771.

(30) Liu, S.; Tong, Z.; Zhao, J.; Liu, X.; Wang, J.; Ma, X.; Chi, C.; Yang, Y.; Liu, X.; Li, Y. Rational Selection of Amorphous or Crystalline V_2O_5 Cathode for Sodium-Ion Batteries. *Phys. Chem. Chem. Phys.* **2016**, *18*, 25645−25654.

(31) Wang, Q.; Hung, P. C.; Lu, S.; Chang, M. B. Catalytic Decomposition of Gaseous PCDD/Fs Over V_2O_5/TiO_2-CNTs Catalyst: Effect of NO and NH_3 Addition. *Chemosphere* **2016**, *159*, 132−137.

(32) Erdohelyi, A.; Solymosi, F. Partial Oxidation of Ethane Over Supported Vanadium Pentoxide Catalysts. *J. Catal.* **1990**, *123*, 31−42.

(33) Wang, Y.; Katsunori, T.; Kyoungho, H. L.; Cao, G. Z. Nanostructured Vanadium Oxide Electrodes for Enhanced Lithium-Ion Intercalation. *Adv. Funct. Mater* **2006**, *16*, 1133−1144.

(34) Dhayal Raj, A.; Pazhanivel, T.; Suresh Kumar, P.; Mangalaraj, D.; Nataraj, D.; Ponpandian, N. Self-Assembled V_2O_5 Nanorods For Gas Sensors. *Curr. Appl. Phys.* **2010**, *10*, 531−537.

(35) Ottaviano, L.; Pennisi, A.; Simone, F.; Salvi, A. M. RF Sputtered Electro Chromic V_2O_5 Films. *Opt. Mater.* **2004**, *27*, 307−313.
(36) Liu, Z.; Guojia, F.; Youqing, W.; Yandong, B.; Kai-Lun, Y. Laser-Induced Colouration of V_2O_5. *J. Phys. D: Appl. Phys.* **2000**, *33*, 2327−2332.
(37) Benmouss, M.; Outzourhit, A.; Jourdani, R.; Bennouna, A.; Ameziane, E. L. Structural, Optical and Electrochromic Properties of Sol−Gel V_2O_5 Thin Films. *Act. Passive Electron. Compon.* **2003**, *26*, 245−256.
(38) Le, H. A.; Chin, S.; Park, E.; Bae, G.; Jurng, J. Chemical Vapor Synthesis and Physico-Chemical Properties of V_2O_5 Nanoparticles. *Chem. Vap. Deposition* **2012**, *18*, 6−9.
(39) Liu, D. Q.; Zheng, W. W.; Cheng, H. F.; Liu, H. T. Thermochromic VO_2 Thin Film Prepared by Post Annealing Treatment of V_2O_5 Thin Film. *Adv. Mater. Res* **2009**, *79*−*82*, 747−750.
(40) Lataste, E.; Demourgues, A.; Salmi, J.; Naporea, C.; Gaudon, M. Thermochromic Behavior (400 < T° C < 1200 °C) of Barium Carbonate/Binary Metal Oxide Mixtures. *Dyes Pigm.* **2011**, *91*, 396−403.
(41) Gaudon, M.; Deniard, P.; Voisin, L.; Lacombe, G.; Darnat, F.; Demourgues, A.; Perillon, J. L.; Jobic, S. How to Mimic the Thermo-Induced Red to Green Transition of Ruby with Control of The Temperature Via the Use of An Inorganic Materials Blend? *Dyes Pigm.* **2012**, *95*, 344−350.
(42) Kumar, S.; Maury, F.; Bahlawane, N. Electrical Switching in Semiconductor-Metal Self-Assembled VO_2 Disordered Metamaterial Coatings. *Sci. Rep.* **2016**, *6*, No. 37699.
(43) Kumar, S.; Lenoble, D.; Maury, F.; Bahlawane, N. Synthesis of Vanadium Oxide Films with Controlled Morphologies: Impact on the Metal−Insulator Transition Behavior. *Phys. Status Solidi A* **2015**, *212*, 1582−1587.
(44) Rampelberg, G.; Schutter, B.; Devulder, W.; Martens, K.; Radu, I.; Detavernier, C. In Situ X-Ray Diffraction Study of the Controlled Oxidation and Reduction in the V−O System for the Synthesis of VO_2 And V_2O_3 Thin Films. *J. Mater. Chem. C* **2015**, *3*, 11357−11365.
(45) Bahlawane, N.; Lenoble, D. Vanadium Oxide Compounds: Structure, Properties, and Growth from the Gas Phase. *Chem. Vap. Deposition* **2014**, *20*, 299−311.
(46) Su, Q.; Liu, X. Q.; Ma, H. L.; Guo, Y. P.; Wang, Y. Y. Raman Spectroscopic Characterization of the Microstructure of V_2O_5 Films. *J. Solid State Electrochem.* **2008**, *12*, 919−923.
(47) Haber, J.; Witko, M.; Tokarz, R. Vanadium Pentoxide I. Structures and Properties. *Appl. Catal., A* **1997**, *157*, 3−22.
(48) Zhou, B.; Deyan, H. Raman Spectrum of Vanadium Pentoxide from Density-Functional Perturbation Theory. *J. Raman Spectrosc.* **2008**, *39*, 1475−1481.
(49) Kang, M.; Kim, I.; Kim, S.; Ryu, J.-W.; Park, H. Metal-Insulator Transition Without Structural Phase Transition in V_2O_5 Film. *Appl. Phys. Lett.* **2011**, *98*, No. 131907.
(50) Blum, R.-P.; Niehus, H.; Hucho, C.; Fortrie, R.; Ganduglia-Pirovano, M.; Sauer, J.; Shaikhutdinov, S.; Freund, H. Surface Metal-Insulator Transition on a Vanadium Pentoxide (001) Single Crystal. *Phys. Rev. Lett.* **2007**, *99*, No. 226103.
(51) Fisher, B.; Genossar, J.; Patlagan, L.; Chashka, K. B.; Reisner, G. M. Electric-Field-Induced Semiconductor−Semiconductor Transition in V_2O_5. *Appl. Phys. A: Mater. Sci. Process.* **2015**, *120*, 435−442.
(52) Pergament, A. L.; Stefanovich, G. B.; Kuldin, N. A.; Velichko, A. A. On the Problem of Metal-Insulator Transitions in Vanadium Oxides. *ISRN Condens. Matter Phys.* **2013**, No. 960627.
(53) Aita, C.; Liu, Y.-L.; Kao, M.; Hansen, S. Optical Behavior of Sputter-Deposited Vanadium Pentoxide. *J. Appl. Phys.* **1986**, *60*, 749−753.